Spin waves in the anisotropic fcc kagome antiferromagnet

M. D. LeBlanc,[1] B. W. Southern,[2] M. L. Plumer,[1] and J. P. Whitehead[1]

[1]*Department of Physics and Physical Oceanography, Memorial University of Newfoundland, St. John's, Newfoundland, Canada A1B 3X7*

[2]*Department of Physics and Astronomy, University of Manitoba, Winnipeg, Manitoba, Canada R3T 2N2*

(Received 28 February 2014; revised manuscript received 22 August 2014; published 2 October 2014)

Classical spin-wave calculations demonstrate that the macroscopic continuous degeneracy associated with the two-dimensional kagome Heisenberg spin lattice persists in the case of the stacked fcc structure, giving rise to zero-energy modes in three dimensions. The addition of an effective local cubic anisotropy is shown to remove this continuous degeneracy and introduce a gap in the spectrum as well as modify the inelastic scattering function $S(\mathbf{q},\omega)$. This scenario supports earlier Monte Carlo simulations which indicate that the phase transition to long-range $q = 0$ magnetic order is driven to be discontinuous by critical fluctuations associated with the large degeneracy in the absence of anisotropy but becomes continuous with the addition of anisotropy. The results are relevant to Ir-Mn alloys, which are widely used in the magnetic storage industry in thin-film form as the antiferromagnetic pinning layer in spin-valve structures.

DOI: 10.1103/PhysRevB.90.144403 PACS number(s): 75.30.Ds, 75.30.Gw, 75.50.Ee

I. INTRODUCTION

The classical Heisenberg model on an isolated two-dimensional (2D) kagome layer with nearest-neighbor antiferromagnetic exchange interactions is an example of a fully frustrated magnetic system with a macroscopically degenerate ground state of 120° spin structures on corner-sharing triangles, known as $q = 0$ magnetic order [1]. This extensive degeneracy is accompanied by the presence of zero-energy spin-wave excitations which can take the system from one ground state to another [2,3]. Evidence for such a mode through inelastic neutron scattering experiments has been reported in a system with weakly coupled kagome layers [4]. (More exotic ground states have also been predicted to occur in the 2D kagome spin lattice when quantum effects are important [5].) Zero-energy (classical) modes also occur in the stacked triangular lattice antiferromagnet where the interlayer exchange coupling J' differs from the intralayer interaction J (a model of the magnetism in solid oxygen) [6,7]. In this case of rhombohedral symmetry, the degeneracy is associated with ground-state helimagnetism and occurs if $|J'| < 3|J|$. For this system, degenerate modes occur along lines in reciprocal space that are dependent on the value of J'. Similar macroscopic degeneracies are found in spin-ice materials [8–11] and can often be lifted by thermal or quantum fluctuations through the mechanism of order by disorder in which states are selected from the ground-state manifold by entropic forces [12,13]. Such degeneracies can also be removed with the addition of further neighbor interactions or magnetic anisotropies [4,6,14].

Monte Carlo simulations have recently been reported on three-dimensional (3D) kagome Heisenberg and XY spin systems composed of stacked layers with fcc symmetry (see Fig. 1) [15]. The results suggest that continuous macroscopic degeneracy associated with the 2D system persists in this 3D spin lattice. The degeneracy in the 3D system does not yield a finite ground-state entropy but scales with the linear size of the system. In the absence of anisotropy, the 3D system exhibits a finite-temperature phase transition that is weakly first order, speculated to be driven so by critical fluctuations associated with the large degree of degeneracy. With the addition of a local cubic anisotropy [16,17], the nature of the transition becomes continuous, a phenomenon also reported in spin-ice materials [9].

The magnetic properties of Ir-Mn alloys have attracted a great deal of interest due to their widespread use as the antiferromagnetic pinning layer in spin-valve devices for magnetic recording [19–21]. Ordered $IrMn_3$, and sister compounds $RhMn_3$ and $PtMn_3$, adopts the $CuAu_3$ crystal structure [22] with magnetic Mn ions on cube faces and nonmagnetic (Ir) ions occupying cube corners. The high Néel temperature of $IrMn_3$ ($T_N = 960$ K) makes it particularly useful for applications that require robustness to thermal fluctuations at device operating temperatures. Despite extensive study of their magnetic structures spanning many decades, including a seminal neutron diffraction work identifying the 120° spin structure, [18] the connection to the kagome structure was not realized until recently [15]. This has inspired a new study of $IrMn_3$ as a possible candidate for observing the anomalous Hall effect in zero applied magnetic field [23]. A recent neutron diffraction study of single-crystal $IrMn_3$ shows that the $q = 0$ spin structure remains for thin films and emphasizes the importance of this frustrated magnetic ordering on the exchange-bias phenomena in this compound [24]. This relationship, and the importance of anisotropy, has also been revealed in recent electronic structure calculations and micromagnetic simulations on $IrMn_3$/Co bilayer thin films [25].

In the present work we examine the spin-wave excitations as well as the scattering intensity function $S(\mathbf{q},\omega)$ of a model Hamiltonian with unequal intraplane and interplane antiferromagnetic exchange interactions including local cubic anisotropy. It is shown that the addition of interplane exchange and anisotropy either reduces or removes the macroscopic degeneracy associated with the 2D kagome system and that this behavior is related to the reduction or removal of the number of zero-energy modes in the excitation spectrum. In addition, the impact of anisotropy on the elastic scattering is also examined. The results provide guidance for the potential observation of these effects through elastic and inelastic neutron diffraction measurements of $IrMn_3$ and its sister compounds.

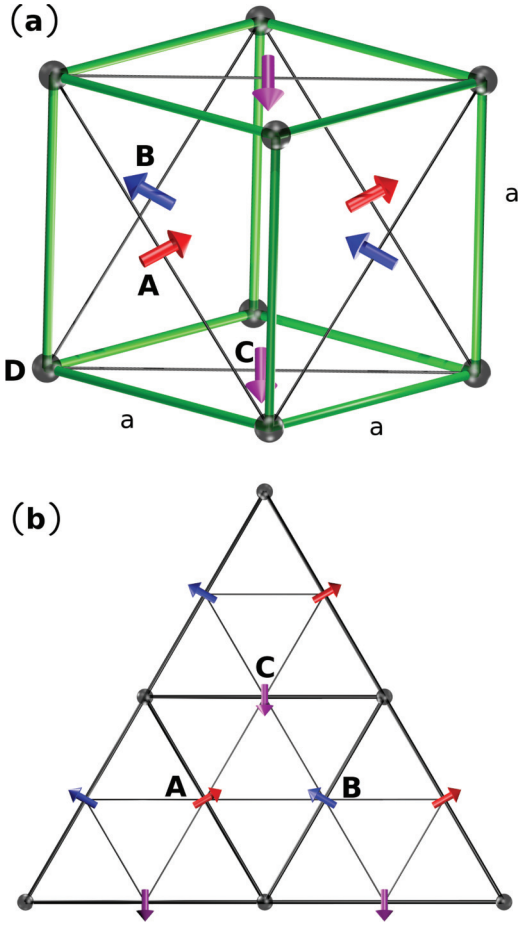

FIG. 1. (Color online) (a) The fcc lattice is divided into four cubic sublattices, labeled A,B,C, and D, each with lattice constant a. The D sites (spheres) are nonmagnetic, whereas the remaining three sublattices (arrows) are magnetic. (b) The A,B, and C sites form a set of kagome lattices stacked along the (111) direction. Adapted from Ref. [18].

II. MODEL

The magnetic ions form an fcc lattice with one of the four cubic sublattices replaced by nonmagnetic sites as shown in Fig. 1. The three remaining sublattices form stacked kagome layers parallel to the [111] directions and are labeled A, B, and C. Each magnetic site has four nearest neighbors (NNs) in the (111) planes and two NNs in each of the planes above and below. We consider NN exchange interactions as well as a local cubic anisotropy described by the Hamiltonian

$$\mathcal{H} = J \overset{\text{intraplane}}{\sum_{i<j}} \mathbf{S}_i \cdot \mathbf{S}_j + J' \overset{\text{interplane}}{\sum_{i<j}} \mathbf{S}_i \cdot \mathbf{S}_j - K \sum_{\gamma} \sum_{l \subset \gamma} (\mathbf{S}_l \cdot \mathbf{n}_\gamma)^2, \tag{1}$$

where $J > 0$ is the antiferromagnetic coupling to the four in-plane NNs, $J' \geqslant 0$ couples the four out-of-plane NN spins, and the anisotropy $K \geqslant 0$ has a different easy direction for each of the three sublattices. Here, γ represents sublattices A, B, and C, l is summed over the $\frac{N}{3}$ spins of sublattice γ, $\mathbf{S}_i$ are unit classical Heisenberg spin vectors at each site, and $\mathbf{n}_\gamma$ are unit vectors in the cube axis directions, $\mathbf{n}_\mathrm{A} = \hat{\mathbf{x}}$, $\mathbf{n}_\mathrm{B} = \hat{\mathbf{y}}$, and $\mathbf{n}_\mathrm{C} = \hat{\mathbf{z}}$. Electronic structure calculations [17] have been used to estimate $K/J \approx 0.1$ in the case of $IrMn_3$.

For zero anisotropy, the ground state is a planar configuration with the sum of the spins on each elementary triangle $\mathbf{S}_A + \mathbf{S}_B + \mathbf{S}_C = 0$. For decoupled kagome planes ($J' = 0$) there is an extensive ground-state degeneracy which includes both periodic and nonperiodic ground states. Previous spin-wave calculations at zero temperature for the $q = 0$ and $\sqrt{3}\times\sqrt{3}$ periodic ground states find zero-energy dispersionless modes which are related to the macroscopic degeneracy [2]. The decoupled kagome planes do not order at a finite temperature but are believed to select a planar arrangement of the spins as $T \to 0$, and spin dynamic simulations indicate strong $\sqrt{3}\times\sqrt{3}$ spin correlations at low T [3,26]. For coupled planes ($J' > 0$), there is a finite-temperature phase transition to the $q = 0$ state which is weakly first order [15]. The ground-state degeneracy is no longer extensive, but there are continuous rotations of two of the three sublattices which do not change the energy and correspond to local modes. When the cubic anisotropy is added, particular spin planes are selected, and all of the macroscopic degeneracy is removed with the phase transition changing from first order to second order.

The effect of the cubic anisotropy can be studied by defining α as the cosine of the angle between each sublattice spin and its anisotropy axis [$\alpha = \cos(\boldsymbol{S}_i \cdot n_i)$, $i =$ A, B, C] and β as the cosine of the angle with respect to the other two anisotropy axes [$\beta = \cos(\boldsymbol{S}_i \cdot n_j)$, $i \neq j$], where $\alpha^2 + 2\beta^2 = 1$ for spins of unit length. The ground-state energy per spin is given by

$$E/N = 2(J + J')(\beta^2 - 2\alpha\beta) - K\alpha^2 \tag{2}$$

and is minimized when α has the value

$$\alpha = \sqrt{1/2 + 1/2\sqrt{1 - 1/[1 + (\tilde{K} + 1)^2/8]}}, \tag{3}$$

where $\tilde{K} = K/(J + J')$ and $\beta = \sqrt{\frac{1-\alpha^2}{2}}$ using the positive values of the square roots to give physical solutions. For $K = 0$, $\alpha = 2\beta = 2/\sqrt{6}$, which describes spins in the coplanar 120° spin structure which can have an arbitrary orientation with respect to the crystal axes. However, when $K > 0$, the spins are no longer coplanar and have a net moment per site directed out of the (111) plane with magnitude $(\alpha - 2\beta)/\sqrt{3}$. There are eight possible ground states corresponding to the (111) planes with the spins being lifted out of the plane, resulting in a net magnetization along one of the [111] axes [16].

III. SPIN WAVES

In order to study the linearized spin-wave excitations, we consider a single domain in which the net magnetization is along the positive [111] direction. The spins $\mathbf{S}_i$ on each sublattice are transformed to local spin coordinates $\tilde{\mathbf{S}}_i$ such that $\tilde{S}_i^z = 1$ in the ground state. We look for plane-wave solutions involving the transverse spin components $\tilde{\mathbf{S}}_i = \tilde{\mathbf{S}} e^{i(\mathbf{k}\cdot\mathbf{r}_i - \omega t)}$, and the linearized equations for the six transverse spin amplitudes can be obtained through the standard torque equation [27] or

other techniques [28], given by

$$-i\omega\begin{pmatrix}\tilde{S}^x_A\\ \tilde{S}^x_B\\ \tilde{S}^x_C\\ \tilde{S}^y_A\\ \tilde{S}^y_B\\ \tilde{S}^y_C\end{pmatrix}=\begin{pmatrix}0 & Y_{AB} & -Y_{AC} & X & Z_{AB} & Z_{AC}\\ -Y_{AB} & 0 & Y_{BC} & Z_{AB} & X & Z_{BC}\\ Y_{AC} & -Y_{BC} & 0 & Z_{AC} & Z_{BC} & X\\ W & T_{AB} & T_{AC} & 0 & Y_{AB} & -Y_{AC}\\ T_{AB} & W & T_{BC} & -Y_{AB} & 0 & Y_{BC}\\ T_{AC} & T_{BC} & W & Y_{AC} & -Y_{BC} & 0\end{pmatrix}\begin{pmatrix}\tilde{S}^x_A\\ \tilde{S}^x_B\\ \tilde{S}^x_C\\ \tilde{S}^y_A\\ \tilde{S}^y_B\\ \tilde{S}^y_C\end{pmatrix}, \tag{4}$$

where

$$\begin{aligned}X&=4(J+J')(\beta-2\alpha)\beta-2K\alpha^2,\\ W&=4(J+J')(2\alpha-\beta)\beta+2K(\alpha^2-2\beta^2),\\ Y_{ij}&=(\beta-\alpha/2)\lambda_{ij},\\ Z_{ij}&=\lambda_{ij}/2,\\ T_{ij}&=(2\alpha\beta+\alpha^2/2)\lambda_{ij},\end{aligned} \tag{5}$$

and

$$\begin{aligned}\lambda_{AB}&=2J\cos\left[(k_x-k_y)\frac{a}{2}\right]+2J'\cos\left[(k_x+k_y)\frac{a}{2}\right],\\ \lambda_{BC}&=2J\cos\left[(k_x-k_z)\frac{a}{2}\right]+2J'\cos\left[(k_x+k_z)\frac{a}{2}\right],\\ \lambda_{AC}&=2J\cos\left[(k_y-k_z)\frac{a}{2}\right]+2J'\cos\left[(k_y+k_z)\frac{a}{2}\right].\end{aligned} \tag{6}$$

The wave-vector components k_x,k_y,k_z are defined with respect to the cubic axes with lattice constant a. The linearized equations yield real eigenvalues $\pm\omega_1,\pm\omega_2,\pm\omega_3$. In the general case, these values must be obtained numerically, but analytic results can be determined in special cases.

A. Zero anisotropy

For $K=0$, the ground state is the planar spin configuration with the three sublattices oriented at 120° with respect to each other. In this case the problem can be reduced to finding the eigenvalues ω^2 of a 3×3 symmetric matrix

$$\begin{pmatrix}A_1 & B_1 & B_2\\ B_1 & A_2 & B_3\\ B_2 & B_3 & A_3\end{pmatrix}, \tag{7}$$

where

$$\begin{aligned}A_1&=4(J+J')^2-\left(\lambda^2_{AB}+\lambda^2_{AC}\right)/2,\\ A_2&=4(J+J')^2-\left(\lambda^2_{AB}+\lambda^2_{BC}\right)/2,\\ A_3&=4(J+J')^2-\left(\lambda^2_{AC}+\lambda^2_{BC}\right)/2,\\ B_1&=(J+J')\lambda_{AB}-\lambda_{AC}\lambda_{BC}/2,\\ B_2&=(J+J')\lambda_{AC}-\lambda_{AB}\lambda_{BC}/2,\\ B_3&=(J+J')\lambda_{BC}-\lambda_{AB}\lambda_{AC}/2.\end{aligned} \tag{8}$$

If the interplane coupling J' is also zero, λ_{ij} satisfy the following relation for arbitrary values of the wave vector $\boldsymbol{k}$:

$$\lambda^2_{AB}+\lambda^2_{BC}+\lambda^2_{AC}=4J^2+\lambda_{AB}\lambda_{BC}\lambda_{AC}/J. \tag{9}$$

The characteristic cubic equation has a zero eigenvalue for all $\mathbf{k}$, and the remaining two eigenvalues are degenerate and given by the following expressions:

$$\begin{aligned}\omega_1&=0,\\ \omega_{2,3}&=\sqrt{2}J\{\sin[(k_x-k_y)a/2]^2+\sin[(k_x-k_z)a/2]^2\\ &\quad+\sin[(k_y-k_z)a/2]^2\}^{1/2},\end{aligned} \tag{10}$$

where the wave-vector components k_x,k_y,k_z are defined with respect to the cubic axes with lattice constant a. These expressions agree with previous results [2] for the NN $q=0$ kagome spin lattice when $a=\sqrt{2}$ (corresponding to a NN distance of unity). The dispersionless mode is related to the local rotations of the spins from one ground state to another. Note that for $k_x=k_y=k_z$ all three modes are dispersionless. The latter case corresponds to the fact that the decoupled kagome planes can have arbitrary uniform rotations with respect to one another. For $\mathbf{k}$ along one of the cube axes, Eq. (10) reduces to $\omega_2=\omega_3=2J|\sin(ka/2)|$.

When the interplane interaction $J'>0$, the cubic characteristic equation again factors if any two λ_{ij} are equal, such as when $k_y=k_z$. In this particular case we have $A_1=A_3$ and $B_1=B_3$, and the eigenvalues are

$$\begin{aligned}\omega^2_1&=A_1-B_2,\\ \omega^2_{2,3}&=\frac{A_1+A_2+B_2}{2}\pm\frac{\sqrt{(A_1-A_2+B_2)^2+8B_1^2}}{2}.\end{aligned} \tag{11}$$

Similar expressions can be obtained for $k_x=k_y$ or $k_x=k_z$. In general, all three modes are dispersive and nondegenerate when $J'>0$. However, there are two special cases where degeneracy occurs and where zero-frequency modes are present.

For $k_x=k_y=k_z$, analysis shows that

$$\begin{aligned}\omega^2_1=\omega^2_3&=[1-\cos(k_xa)][4J'^2+6JJ'+2J'^2\cos(k_xa)],\\ \omega^2_2&=[1-\cos(k_xa)][4J'^2+12JJ'+8J'^2\cos(k_xa)].\end{aligned} \tag{12}$$

All three modes are dispersive due to the coupling between kagome planes, and two are degenerate. However, note that ω_2 becomes a soft mode at the zone boundary $k_x=\pi/a$ when $J'=3J$. For values of the interplane coupling $J'>3J$ the ground state is no longer the $q=0$ kagome state but rather corresponds to ferromagnetic kagome planes which are ordered antiferromagnetically with respect to each other. In this paper we restrict our considerations to $J'<3J$.

In the second special case, $k_y=k_z=0$, which corresponds to spin waves propagating parallel to one of the cubic crystal

axes, we have

$$\omega_1 = 0,$$
$$\omega_2 = \omega_3 = 2(J + J')|\sin(ka/2)|, \quad (13)$$

where k represents k_x,k_y, or k_z. These expressions reduce to the correct 2D result above when $J' = 0$. Hence, the coupling of the planes stiffens the excitations for wave vectors along the crystal axes but does not remove the zero-frequency mode.

The zero mode can be understood from Fig. 1. The $x = na$ planes only have B sites, whereas the $x = (n + 1/2)a$ planes have both A and C sites, where $n = 0,1,2,\ldots$. In the ground state the A and C sublattices are at 120° to each other and to the B sublattice. The entire plane of AC spins can be rotated continuously about the direction of the B sublattice spins in the planes on either side with no change in energy. In addition, these rotations in each of the AC planes are independent and correspond to a set of localized excitations for $J + J' > 0$. When $J' = 0$, there are additional degeneracies which lead to a zero-energy mode [2] for all **k**.

B. Effects of anisotropy

In the general case with $K > 0$, the spin-wave frequencies can only be obtained numerically. The ground state is no longer a planar configuration, the continuous degeneracies are removed, and there are no zero modes. For values of **k** along the cubic axes, the lowest mode is almost dispersionless, while the other two modes have strong dispersion. In all other wave-vector directions, all three modes have strong dispersion. Figure 2 shows the spin-wave frequencies ω along the $\Gamma X(100)$ and $\Gamma R(111)$ directions for different values of the interplane coupling J' and the cubic anisotropy K. For $K = 0$, the effect of J' is to stiffen the frequencies along ΓX and to remove the zero modes along ΓR. For $K > 0$, the zero modes along both ΓX and ΓR now have a substantial gap. Along the ΓX direction, there is a low-frequency mode which is almost dispersionless (similar to the mode reported in Ref. [4]). Based on electronic structure calculations [17], the case $K = 0.1J$ with $J' = J$ best represents $IrMn_3$. As shown in the next section, there is a strong dependence of the inelastic scattering intensity on the wave vector.

At the zone center $\mathbf{k} = \mathbf{0}$ we can obtain the leading behavior of the three positive frequencies as a function of K,

$$\omega_1 \simeq \omega_2 \simeq \sqrt{2(J + J')K},$$
$$\omega_3 \simeq 2\sqrt{2(J + J')K}. \quad (14)$$

Hence, all modes have a gap for $K > 0$, and although ω_1,ω_2 are degenerate to leading order in K, they become nondegenerate as K increases. At point R ($k_x = k_y = k_z = \pi/a$) and with $J' = J$, all three modes are degenerate for all K.

In our previous Monte Carlo simulations [16], the sublattice magnetizations did not saturate at low T and displayed evidence of degenerate spin configurations at $T = 0$ for values of K/J smaller than ~0.06. This behavior is consistent with the presence of a small gap in the excitation spectrum. As K increases, the gap increases, and the sublattices become fully saturated as $T = 0$ is approached.

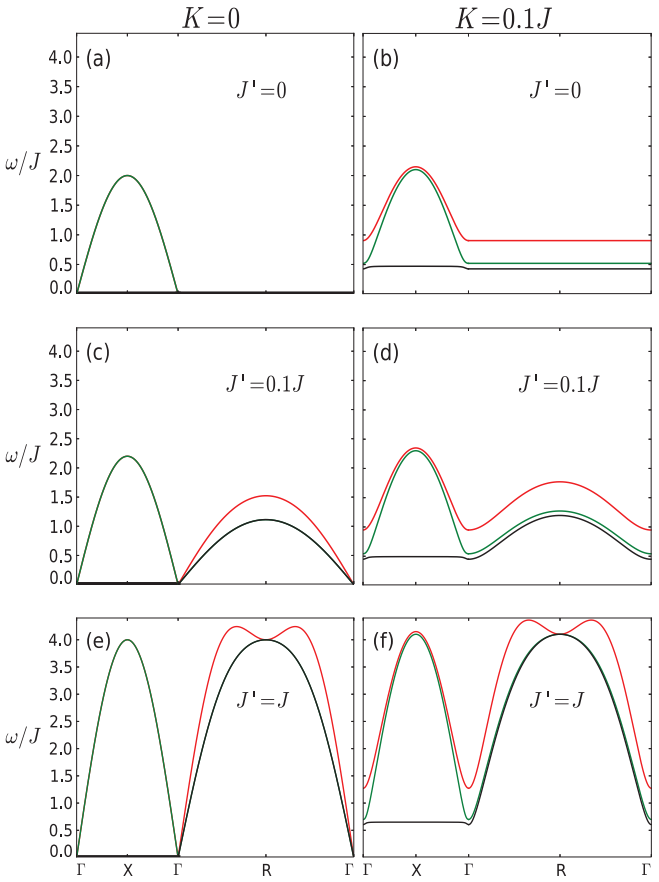

FIG. 2. (Color online) Spin-wave modes along the ΓX and ΓR directions: (a) $K = 0, J' = 0$, (b) $K = 0.1J, J' = 0$, (c) $K = 0$, $J' = 0.1J$, (d) $K = 0.1J, J' = 0.1J$, (e) $K = 0, J' = J$, and (f) $K = 0.1J, J' = J$.

IV. NEUTRON SCATTERING

The effect of the cubic anisotropy can be studied using elastic and inelastic magnetic neutron scattering. Here we consider the case of a single magnetic domain at zero temperature as above.

A. Elastic scattering

The elastic magnetic scattering intensity is proportional to the quantity [29]

$$I(h,k,l) = |F(\vec{\kappa})|^2 \sum_{m,n=x,y,z} S^{mn}(\vec{\kappa})(\delta_{mn} - \hat{\kappa}_m\hat{\kappa}_n), \quad (15)$$

where $F(\vec{\kappa})$ is the magnetic form factor and $S^{mn}(\vec{\kappa})$ is the static magnetic structure factor, with $\vec{\kappa} = \frac{2\pi}{a}(h,k,l)$ being the scattering vector. For zero anisotropy, the spins have a 120° structure and lie in the (111) plane, but for $K > 0$ the spins are nonplanar, and each has a component along the [111] direction, leading to a nonzero magnetization [16]. The value of $I(h,k,l)$ depends on the direction of $\vec{\kappa}$ with respect to the [111] direction. For zero anisotropy, there are no contributions from h,k,l when they are all even or all odd whereas for $K > 0$ these terms become nonzero and are proportional to the magnetization squared. However, these additional peaks are very small compared to the principal peaks. Figure 3 shows

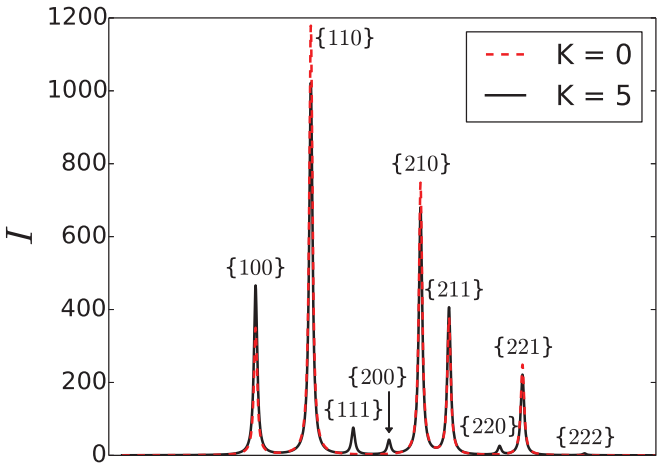

FIG. 3. (Color online) Elastic scattering showing several peaks for $K/J = 0{,}5$ and $J = J' = 1$.

the elastic scattering intensity for $K/J = 0$ and $K/J = 5$ using values of the form factor for Mn ions. These results would be appropriate for a powder sample as all marked peaks correspond to a summation of the multiplicity for a given (hkl). For $K > 0$, other peaks appear in the neutron diffraction, but they would also likely be unobservable for $K = 0.1J$. A more promising signature of anisotropy in $IrMn_3$ may be through inelastic magnetic scattering.

B. Inelastic scattering

Inelastic magnetic scattering is proportional to the dynamic structure factor

$$S(\mathbf{q},\omega) = \sum_{m,n=x,y,z} S^{mn}(\mathbf{q},\omega)(\delta_{mn} - \hat{q}_m\hat{q}_n), \qquad (16)$$

where $S^{mn}(\mathbf{q},\omega)$ is the double Fourier transform of the correlation function $\langle S_i^m(0)S_j^n(t)\rangle$ and can be calculated using the above results for the dispersion relations along with standard Green's functions techniques [29].

Figure 4 shows $S(\mathbf{q},\omega)$ calculated with the assumption of a single magnetic (111) domain at fixed values of $\mathbf{q}$ along [100] directions with $J = J' = 1$ for both $K = 0$ and $K/J = 0.1$. We allow the wave vector to extend beyond the first zone boundary for Figs. 4(a) and 4(b), but restrict it to be in the first zone for Figs. 4(c) and 4(d). In Figs. 4(a) and 4(b), the intensity is very large at wave vectors $\vec{\kappa} = \frac{2\pi}{a}(h,k,l)$, corresponding to the elastic peaks with h,k,l not being all even or odd, but the scale is such that the smaller wave-vector modes [which can be seen in Figs. 4(c) and 4(d)] are not visible due to the large intensity near the elastic peaks located at $\vec{\kappa} = \frac{2\pi}{a}(1,0,0)$. The

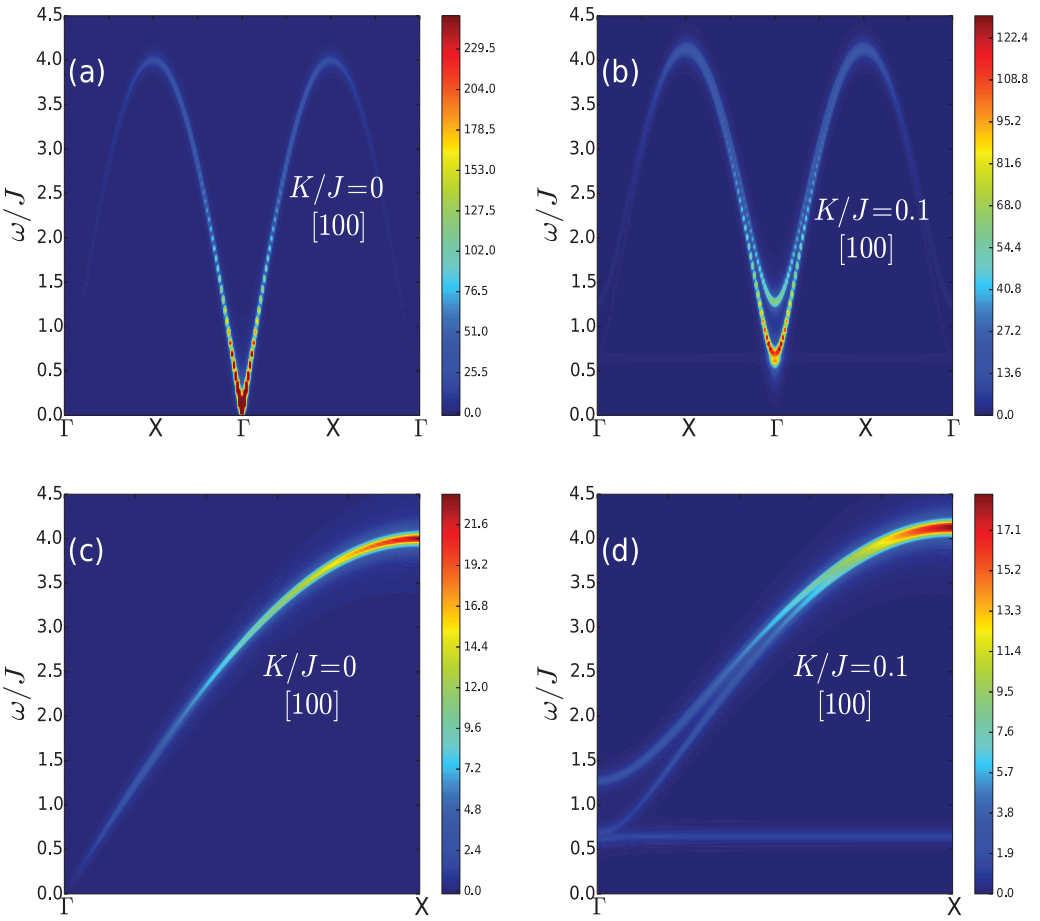

FIG. 4. (Color online) Relative magnitude of the inelastic scattering function $S(\mathbf{q},\omega)$ (side bar scale) assuming a single magnetic (111) domain with $J = J' = 1$ with $\mathbf{q} \parallel [100]$. (a) $K = 0$, (b) $K/J = 0.1$, (c) $K = 0$ over a smaller region than in (a), and (d) $K/J = 0.1$ over a smaller region than in (b).

flat mode is clearly visible in Fig. 4(d) on the smaller scale but has an intensity that is much reduced from the other modes at the zone boundary. Figure 4 can be compared with Figs. 2(e) and 2(f), illustrating the appearance of the low-frequency mode along ΓX and the splitting of the degeneracy of the higher-frequency modes. While the [111] direction (ΓR) is not shown, the intensity is on the order of a hundred times smaller than the [100] direction.

Of particular note for all of the results shown in Fig. 4 is that the intensity is expected to be relatively small in the first Brillouin zone but is substantially larger in the second zone. On comparing Figs. 4(a) and 4(c) with Figs. 4(b) and 4(d), the impact of the anisotropy on the calculated spectrum is very strong.

V. SUMMARY AND CONCLUSIONS

The results of this work have demonstrated that the fcc kagome antiferromagnet is an example of the relatively rare phenomenon of macroscopic continuous degeneracy in 3D that gives rise to zero-energy spin-wave modes. Local cubic anisotropy is found to remove this degeneracy and introduce a gap in the spectrum. The lowest mode at small K is almost dispersionless and has energy $\omega \sim 2\sqrt{JK}$ when $J' = J$, which is about $0.63J$, assuming $K/J \approx 0.1$. The electronic structure calculations [17] on $IrMn_3$ provide the estimate $J \sim 40$ meV, giving $\omega \sim 25$ meV. Anisotropy does not have a significant effect for elastic neutron scattering but induces a uniform magnetization in the [111] direction which could be utilized to stabilize a single-domain sample using field-cooling techniques to better facilitate observation of these effects with inelastic neutron scattering experiments. These results support earlier Monte Carlo simulations which suggest that in the absence of anisotropy critical fluctuations drive the phase transition to be discontinuous but that it becomes continuous with the addition of anisotropy due to the removal of degeneracies. The link between such removal of degeneracy in geometrically frustrated spin systems through anisotropic interactions, the nature of the phase transition to long-range order, and magnetic excitations has recently been established in the pyrochlore antiferromagnet $Er_2Ti_2O_7$ [30]. Degeneracies are known to give rise to critical fluctuations which can drive a phase transition that is continuous within mean-field theory to be first order [31]. In the present system, the introduction of an energy gap in the spin-wave spectrum due to the addition of local cubic anisotropy suppresses the low-energy excitations responsible for the critical fluctuations near the Néel temperature. The model used in the present work can also serve as the foundation for further study of dynamic excitations associated with exchange bias phenomena in bilayer thin films that use $IrMn_3$.

ACKNOWLEDGMENTS

This work was supported by the Natural Sciences and Engineering Council (NSERC) of Canada, the Canada Foundation for Innovation (CFI), and Compute Canada. We thank the referees for their insightful comments.

[1] J. T. Chalker, P. C. W. Holdsworth, and E. F. Shender, Phys. Rev. Lett. **68**, 855 (1992).
[2] A. B. Harris, C. Kallin, and A. J. Berlinsky, Phys. Rev. B **45**, 2899 (1992).
[3] S. Schnabel and D. P. Landau, Phys. Rev. B **86**, 014413 (2012).
[4] K. Matan, D. Grohol, D. G. Nocera, T. Yildirim, A. B. Harris, S. H. Lee, S. E. Nagler, and Y. S. Lee, Phys. Rev. Lett. **96**, 247201 (2006).
[5] S. Yan, D. A. Huse, and S. R. White, Science **332**, 1173 (2011).
[6] E. Rastelli and A. Tassi, J. Phys. C **19**, L423 (1986); **21**, 1003 (1988).
[7] A. P. J. Jansen, Phys. Rev. B **33**, 6352 (1986).
[8] S. T. Bramwell and M. J. P. Gingras, Science **294**, 1495 (2001).
[9] M. E. Zhitomirsky, M. V. Gvozdikova, P. C. W. Holdsworth, and R. Moessner, Phys. Rev. Lett. **109**, 077204 (2012).
[10] A. W. C. Wong, Z. Hao, and M. J. P. Gingras, Phys. Rev. B **88**, 144402 (2013).
[11] K. A. Ross, Y. Qiu, J. R. D. Copley, H. A. Dabkowska, and B. D. Gaulin, Phys. Rev. Lett. **112**, 057201 (2014).
[12] J. Villain, R. Bidaux, J.-P. Carton, and R. Conte, J. Phys. Fr. **41**, 1263 (1980).
[13] C. L. Henley, Phys. Rev. Lett. **62**, 2056 (1989).
[14] F. Shahbazi and S. Mortezapour, Phys. Rev. B **77**, 214420 (2008).
[15] V. Hemmati, M. L. Plumer, J. P. Whitehead, and B. W. Southern, Phys. Rev. B **86**, 104419 (2012).
[16] M. D. LeBlanc, M. L. Plumer, J. P. Whitehead, and B. W. Southern, Phys. Rev. B **88**, 094406 (2013).
[17] L. Szunyogh, B. Lazarovits, L. Udvardi, J. Jackson, and U. Nowak, Phys. Rev. B **79**, 020403(R) (2009).
[18] I. Tomeno, H. N. Fuke, H. Iwasaki, M. Sahashi, and Y. Tsunoda, J. Appl. Phys. **86**, 3853 (1999).
[19] A. E. Berkowitz and K. Takano, J. Magn. Magn. Mater. **200**, 552 (1999); R. L. Stamps, J. Phys. D **33**, R247 (2000); M. Blamire and B. Hickey, Nat. Mater. **5**, 87 (2006).
[20] K. O'Grady, L. E. Fernandez-Outon, and G. Vallejo-Fernandez, J. Magn. Magn. Mater. **322**, 883 (2010).
[21] M. Tsunoda, H. Takahashi, T. Nakamura, C. Mitsumata, S. Isogami, and M. Takahashi, Appl. Phys. Lett. **97**, 072501 (2010).
[22] E. Krén, G. Kádár, L. Pál, J. Sólyom, and P. Szabó, Phys. Lett. **20**, 331 (1966); E. Krén, G. Kádár, L. Pál, J. Sólyom, P. Szabó, and T. Tarnóczi, Phys. Rev. **171**, 574 (1968); A. Sakuma, R. Y. Umetsu, and K. Fukamichi, Phys. Rev. B **66**, 014432 (2002); T. Ikeda and Y. Tsunoda, J. Phys. Soc. Jpn. **72**, 2614 (2003).
[23] H. Chen, Q. Niu, and A. H. MacDonald, Phys. Rev. Lett. **112**, 017205 (2014).
[24] A. Kohn, A. Kovacs, R. Fan, G. J. McIntyre, R. C. C. Ward, and J. P. Goff, Sci. Rep. **3**, 2412 (2013).
[25] R. Yanes, J. Jackson, L. Udvardi, L. Szunyogh, and U. Nowak, Phys. Rev. Lett. **111**, 217202 (2013).
[26] J. N. Reimers and A. J. Berlinsky, Phys. Rev. B **48**, 9539 (1993).

[27] M. L. Plumer, J. Phys. C **17**, 4663 (1984); H. Tanaka, S. Teraoka, E. Kakehashi, K. Ito, and K. Nagata, J. Phys. Soc. Jpn. **57**, 3979 (1988).
[28] R. M. Morra, W. J. L. Buyers, R. L. Armstrong, and K. Hirakawa, Phys. Rev. B **38**, 543 (1988).
[29] W. Marshall and S. W. Lovesey, *Theory of Thermal Neutron Scattering* (Clarendon Press, Oxford, 1971).
[30] M. E. Zhitomirsky, P. C. W. Holdsworth, and R. Moessner, Phys. Rev. B **89**, 140403(R) (2014).
[31] V. Thanh Ngo and H. T. Diep, Phys. Rev. E **78**, 031119 (2008).